bioRxiv preprint doi: https://doi.org/10.1101/2020.07.01.182089; this version posted July 1, 2020. The copyright holder for this preprint (which was not certified by peer review) is the author/funder, who has granted bioRxiv a license to display the preprint in perpetuity. It is made available under aCC-BY-NC-ND 4.0 International license.

A functional overlap between actively transcribed genes and chromatin boundary elements

Caroline L Harrold[1], Matthew E Gosden[1], Lars L P Hanssen[1], Rosa J Stolper[1], Damien J Downes[1], Jelena M. Telenius[1,2], Daniel Biggs[3], Chris Preece[3], Samy Alghadban[3], Jacqueline A Sharpe[1], Benjamin Davies[3], Jacqueline A. Sloane-Stanley[1], Mira T Kassouf[1], Jim R Hughes[1,2], Douglas R Higgs[1]

[1]MRC Weatherall Institute of Molecular Medicine, Radcliffe Department of Medicine, University of Oxford, Oxford, UK.

[2]MRC WIMM Centre for Computational Biology, MRC Weatherall Institute of Molecular Medicine, Radcliffe Department of Medicine, University of Oxford, Oxford, UK.

[3]Wellcome Centre for Human Genetics, Nuffield Department of Medicine, University of Oxford, Oxford, UK.

bioRxiv preprint doi: https://doi.org/10.1101/2020.07.01.182089; this version posted July 1, 2020. The copyright holder for this preprint (which was not certified by peer review) is the author/funder, who has granted bioRxiv a license to display the preprint in perpetuity. It is made available under aCC-BY-NC-ND 4.0 International license.

1 **Abstract**

2

3 Mammalian genomes are subdivided into large (50-2000 kb) regions of chromatin referred to
4 as Topologically Associating Domains (TADs or sub-TADs). Chromatin within an individual
5 TAD contacts itself more frequently than with regions in surrounding TADs thereby directing
6 enhancer-promoter interactions. In many cases, the borders of TADs are defined by
7 convergently orientated boundary elements associated with CCCTC-binding factor (CTCF),
8 which stabilises the cohesin complex on chromatin and prevents its translocation. This delimits
9 chromatin loop extrusion which is thought to underlie the formation of TADs. However, not
10 all CTCF-bound sites act as boundaries and, importantly, not all TADs are flanked by
11 convergent CTCF sites. Here, we examined the CTCF binding sites within a ~70 kb sub-TAD
12 containing the duplicated mouse α-like globin genes and their five enhancers (5'-R1-R2-R3-
13 Rm-R4-α1-α2-3'). The 5' border of this sub-TAD is defined by a pair of CTCF sites.
14 Surprisingly, we show that deletion of the CTCF binding sites within and downstream of the
15 α-globin locus leaves the sub-TAD largely intact. The predominant 3' border of the sub-TAD
16 is defined by a steep reduction in contacts: this corresponds to the transcribed α2-globin gene
17 rather than the CTCF sites at the 3'-end of the sub-TAD. Of interest, the almost identical α1-
18 and α2-globin genes interact differently with the enhancers, resulting in preferential expression
19 of the proximal α1-globin gene which behaves as a partial boundary between the enhancers
20 and the distal α2-globin gene. Together, these observations provide direct evidence that
21 actively transcribed genes can behave as boundary elements.

bioRxiv preprint doi: https://doi.org/10.1101/2020.07.01.182089; this version posted July 1, 2020. The copyright holder for this preprint (which was not certified by peer review) is the author/funder, who has granted bioRxiv a license to display the preprint in perpetuity. It is made available under aCC-BY-NC-ND 4.0 International license.

22 **Significance Statement**

23

24 Mammalian genomes are complex, organised 3D structures, partitioned into Topologically
25 Associating Domains (TADs): chromatin regions that preferentially self-interact. These
26 chromatin interactions are thought to be driven by a mechanism that continuously extrudes
27 chromatin loops, forming structures delimited by chromatin boundary elements and reflecting
28 the activity of enhancers and promoters. Boundary elements bind architectural proteins such as
29 CCCTC-binding factor (CTCF). Previously, an overlap between the functional roles of
30 enhancers and promoters has been shown. However, whether there is overlap between
31 enhancers/promoters and boundary elements is not known. Here, we show that actively
32 transcribed genes can also behave as boundary elements, similar to CTCF boundaries. In both
33 cases, multi-protein complexes bound to these regions may stall the process of chromatin loop
34 extrusion.

bioRxiv preprint doi: https://doi.org/10.1101/2020.07.01.182089; this version posted July 1, 2020. The copyright holder for this preprint (which was not certified by peer review) is the author/funder, who has granted bioRxiv a license to display the preprint in perpetuity. It is made available under aCC-BY-NC-ND 4.0 International license.

35 **Introduction**

36

37 Gene expression throughout development and differentiation is controlled by an interplay
38 between three fundamental *cis*-acting regulatory elements: enhancers, promoters, and
39 boundary elements. Although each type of element is classified by a working definition which
40 enables researchers to establish the syntax of the genome, it is becoming increasingly clear that
41 there is some overlap in the functional roles of these elements as currently defined. For
42 example, some enhancers act as promoters (1-4) and some promoters may also act as enhancers
43 (2, 5-7). Whether enhancers and promoters can also act as boundary elements has been less
44 well studied.

45

46 In mammals, boundary elements are frequently located at the borders of large (~50-2000 kb)
47 regions of chromatin referred to as Topologically Associating Domains (TADs or sub-TADs;
48 self-interacting domains that are nested within larger TADs with a median size of 185 kb) (8-
49 11). TADs are defined as regions of self-interacting chromatin, in that chromatin within a TAD
50 has a higher contact frequency with itself than with regions in surrounding TADs (8, 9, 12).
51 This is thought to ensure that enhancers predominantly interact with promoters present in the
52 same TAD, adding to the specificity of gene regulation. Current models propose that TADs are
53 formed by the extrusion of chromatin loops via translocation of the cohesin complex (13-15).
54 Importantly, boundary elements recruit the zinc finger CCCTC-binding factor (CTCF) which
55 interrupts the translocation of cohesin in an orientation dependent manner and stabilises this
56 protein complex on chromatin. Consistent with this model, cohesin has been shown to be
57 enriched at active boundary elements (16-20). Deletion or inversion of boundary elements
58 often alters the extent of self-interacting TADs and may enable the formation of new enhancer-
59 promoter contacts often producing aberrant gene regulation (9, 15, 21-30).

60

61 Despite this coherent model integrating the role of enhancers, promoters, and boundary
62 elements which relates genome structure to gene expression, not all CTCF-bound sites act as
63 boundaries (8) and, importantly, not all TADs are flanked by convergent CTCF sites (11, 24).
64 For example, deletion of a CTCF-rich region in the *Firre* locus found that its TAD boundary
65 is preserved, providing evidence for CTCF-independent boundaries (31). Global depletion of
66 CTCF results in a loss (32, 33) or weakening (34) of ~80% of TADs across the genome; but
67 not all TADs depend on CTCF. Of interest, removal of CTCF does not lead to widespread mis-
68 regulation of gene expression (32, 33). Together, these observations suggest that elements other

bioRxiv preprint doi: https://doi.org/10.1101/2020.07.01.182089; this version posted July 1, 2020. The copyright holder for this preprint (which was not certified by peer review) is the author/funder, who has granted bioRxiv a license to display the preprint in perpetuity. It is made available under aCC-BY-NC-ND 4.0 International license.

69 than CTCF binding sites might act as functional boundaries. Previous reports have proposed
70 that actively transcribed genes may play such a role. First, Transcriptional Start Sites (TSSs)
71 of housekeeping genes are enriched at TAD borders (8, 35) and, second, the act of transcription
72 can affect 3D genome structure independently of CTCF (36-38). However, whether an actively
73 transcribed gene can behave as a boundary, in a similar manner to a CTCF element, has not
74 been previously tested in mammalian systems.
75
76 The duplicated mouse α-like globin genes (*Hba-α1* and *Hba-α2*) and their five enhancers (R1,
77 R2, R3, Rm, and R4) form a very well-characterised, small ~70 kb tissue-specific sub-TAD in
78 erythroid cells, arranged 5'-R1-R2-R3-Rm-R4-*Hba-α1-Hba-α2*-3'. In the past, this locus has
79 been extensively used to establish the principles underpinning mammalian gene regulation and
80 relating genome structure to function (26, 39-44). The α-globin sub-TAD is flanked by several,
81 largely convergent CTCF binding sites (26). We have previously shown that *in vivo* deletion
82 of two CTCF binding sites at the upstream border of the α-globin locus results in an expansion
83 of the sub-TAD and the incorporation of three upstream genes into a newly formed sub-TAD.
84 These three genes become upregulated in erythroid cells via interactions with the α-globin
85 enhancers (26). Therefore, the intact 5' boundary normally delimits enhancer interactions and
86 thereby contributes to tissue-specific regulation of gene regulation. However, it is not known
87 which, if any, of the regulatory elements produce a similar boundary at the 3' limit of the
88 α-globin sub-TAD.
89
90 To investigate the boundary elements within and downstream of the sub-TAD, we used
91 CRISPR-Cas9 mediated targeting to generate mouse models with mutations of relevant CTCF
92 binding sites. Specific CTCF sites were targeted individually and in informative combinations.
93 We found that the 3' border of the TAD is only minimally affected by inactivation of any of
94 the tested CTCF sites either individually or in combination. Rather, this border is
95 predominantly defined by the actively transcribed downstream α2-globin gene (*Hba-α2*). In
96 addition, we found that, when transcribed, the upstream α1-globin gene (*Hba-α1*) acts as a
97 partial barrier to enhancer-promoter interactions with the downstream α2-globin gene.
98 Together our findings demonstrate that actively transcribed genes themselves may behave as
99 boundary elements.

bioRxiv preprint doi: https://doi.org/10.1101/2020.07.01.182089; this version posted July 1, 2020. The copyright holder for this preprint (which was not certified by peer review) is the author/funder, who has granted bioRxiv a license to display the preprint in perpetuity. It is made available under aCC-BY-NC-ND 4.0 International license.

100 **Results**

101

102 Deletion of downstream CTCF sites results in only minor expansion of the self-interacting
103 α-globin sub-TAD with no changes in gene expression

104

105 We have previously characterised the sequence and orientation of 16 CTCF binding sites
106 within and flanking the mouse α-globin locus (26). In general, the sub-TAD is flanked by
107 convergently orientated sites (Figure 1). Using NG Capture-C (hereafter referred to as Capture-
108 C) in erythroid cells, we have previously shown and confirm here (Figure 1) that two CTCF
109 binding sites (HS+44/+48) at the 3' end of the α-globin locus display diffuse, weak interactions
110 with the two CTCF-bound sites (HS-38/-39) that constitute the upstream (5') boundary of the
111 sub-TAD (26). These CTCF sites do not interact at all with the active enhancer elements (R1-
112 R4 & Rm) within the α-globin sub-TAD. Therefore, we initially considered that HS+44/+48
113 might delimit the interactions of the α-globin enhancers with promoters lying downstream of
114 the sub-TAD in a similar way to that of HS-38/-39 at the upstream border. We therefore used
115 CRISPR-Cas9 mediated mutagenesis to generate mice with deletions in the binding sequences
116 of these two CTCF sites (Δ44-48; Figure 1 and Supplementary Figure 1a).

117

118 In erythroid cells, isolated from the spleens of homozygous Δ44-48 mice, mutations of the
119 HS+44/+48 binding sequences resulted in a complete loss of CTCF binding at these sites
120 without affecting CTCF binding to other, nearby sites (Figure 1a). In addition, other than the
121 loss of peaks at the deleted CTCF sites, the chromatin accessibility around the α-globin locus
122 in Δ44-48 erythroid cells remained unaltered when compared to wild-type (WT) erythroid
123 cells, indicating that other tissue-specific regulatory elements remained intact and unaltered.
124 To investigate whether the removal of the HS+44/+48 sites resulted in changes in local genome
125 topology, we performed Capture-C from viewpoints across the α-globin locus in WT and
126 Δ44-48 primary erythroid cells. Capture-C profiles from the viewpoint of the functional
127 upstream boundary (CTCF site HS-38) show that in absence of CTCF binding to the
128 HS+44/+48 sites, the diffuse interactions over the downstream sites had shifted to the next pair
129 of downstream CTCF binding sites (HS+65/+66), resulting in a minor expansion of the sub-
130 TAD (Figure 1a). Moreover, Capture-C profiles from the viewpoint of the R1 enhancer showed
131 that this shift was accompanied by only slightly increased interactions between R1 and the
132 region of chromatin downstream of the deleted HS+44/+48 sites. This region does not contain
133 any regulatory elements, showing that this expansion occurs even without the formation of new

bioRxiv preprint doi: https://doi.org/10.1101/2020.07.01.182089; this version posted July 1, 2020. The copyright holder for this preprint (which was not certified by peer review) is the author/funder, who has granted bioRxiv a license to display the preprint in perpetuity. It is made available under aCC-BY-NC-ND 4.0 International license.

134 interactions between defined *cis*-regulatory elements (Supplementary Figure 2). Importantly,
135 the altered local chromatin interactions in Δ44-48 erythroid cells were not accompanied by any
136 changes in local gene expression. The two genes directly downstream of the α-globin locus
137 (*Sh3pxd2b* and *Ubtd2*) are not expressed in WT primary erythroid cells, and RT-qPCR analysis
138 found no detectable difference in expression of *Sh3pxd2b*, *Ubtd2*, or *Hba-α1/2* in Δ44-48
139 erythroid cells when compared to WT erythroid cells (Figure 1b).
140
141 Taken together, these findings show that rather than behaving as a strong boundary element,
142 the HS+44/+48 CTCF sites behave as a minor boundary to loop extrusion and the potential for
143 chromatin interactions. However, unlike the previously characterised 5' boundary and other
144 boundaries described in the literature (9, 15, 22-24, 26, 27, 29, 30), removal of these CTCF
145 sites does not lead to any changes in gene expression within or flanking the α-globin gene
146 cluster.
147
148
149 <u>The actively transcribed α2-globin gene acts as the downstream boundary of the α-globin sub-</u>
150 <u>TAD</u>
151
152 Since the HS+44/+48 sites do not constitute the 3' boundary of the α-globin sub-TAD, we next
153 considered the more proximal CTCF sites that coincide with the θ1/2 genes (*Hbq1b* and
154 *Hbq1a*) (Figure 1), which are situated inside the α-globin sub-TAD and within the duplicated
155 region of the α-globin locus. The θ1/2 genes are α-like genes of unknown function (45). In
156 addition to displaying diffuse interactions with the downstream HS+44/+48 sites, the upstream
157 (5') boundary of the α-globin sub-TAD also diffusely interacts with the θ1/2 CTCF-bound sites
158 (26) (Figure 1). Furthermore, we have previously shown that Capture-C interaction profiles
159 from the viewpoint of any active regulatory element inside the undisturbed sub-TAD display a
160 pronounced reduction in interactions immediately downstream of the 3' α2-globin gene
161 (*Hba-α2*), which, within the resolution of these studies, appears to coincide with the θ2 CTCF
162 binding site (26, 39-41). Therefore, it seemed possible that this CTCF-bound site could act as
163 the 3' boundary of the α-globin sub-TAD. To investigate the roles of CTCF sites inside an
164 active sub-TAD with respect to genome structure and gene regulation, we used CRIPSR-Cas9
165 mediated mutagenesis to generate mice with deletions at the θ CTCF sites individually or in
166 combination (Δθ1, Δθ2, and Δθ1θ2; Figure 2, Figure 3, Supplementary Figure 1b, and
167 Supplementary Figure 3).

bioRxiv preprint doi: https://doi.org/10.1101/2020.07.01.182089; this version posted July 1, 2020. The copyright holder for this preprint (which was not certified by peer review) is the author/funder, who has granted bioRxiv a license to display the preprint in perpetuity. It is made available under aCC-BY-NC-ND 4.0 International license.

168
169 We therefore next analysed primary erythroid cells from Δθ1, Δθ2, and Δθ1θ2 homozygous
170 mice and showed that mutations of the CTCF binding sequences resulted in a complete loss of
171 CTCF binding at the specifically targeted sites (Figure 2, Figure 3, and Supplementary Figure
172 3). Again, there were no additional changes in chromatin accessibility around the α-globin
173 locus in erythroid cells derived from any of the three θ mouse models when compared to WT
174 erythroid cells (Figure 2, Figure 3, and Supplementary Figure 3). To investigate whether
175 removal of CTCF sites within and immediately downstream of the active α-globin locus caused
176 changes to the sub-TAD structure, we performed Capture-C from the viewpoint of the α-globin
177 promoters in WT, Δθ2, and Δθ1θ2 primary erythroid cells. Surprisingly, in both Δθ2 and Δθ1θ2
178 erythroid cells, the 3' boundary of the sub-TAD remained largely intact, and the pronounced
179 reduction in chromatin interactions downstream of the α2-globin gene persisted, despite the
180 loss of CTCF binding at θ2 and both θ sites, respectively (Figure 2; grey arrows). In addition,
181 the overall sub-TAD structure remained largely unaffected. Hence, the θ1/2 CTCF binding
182 sites are not essential to form the 3' boundary of the sub-TAD and these results show that the
183 3' boundary of the sub-TAD is marked by the active α2-globin gene itself.
184
185
186 <u>Investigating the role of CTCF sites lying within the α-globin sub-TAD in regulating gene</u>
187 <u>expression</u>
188
189 Although the CTCF sites lying close by and in between the α-globin genes play no role in
190 forming the 3' boundary of the α-globin sub-TAD, we considered whether they might play a
191 role in fine tuning gene expression within the sub-TAD. In human, the upstream 5' α-globin
192 gene (*HBA2*; the equivalent of mouse *Hba-α1*) is located closer to the enhancers and is more
193 highly expressed than the downstream 3' α-globin gene (*HBA1*; the equivalent of mouse
194 *Hba-α2*). *HBA2* produces ~70% of the total α-globin mRNA (46-48). To determine if this
195 differential expression of the α-globin genes also holds true for mouse, we performed Poly(A)+
196 RNA-seq on primary WT erythroid cells. The presence of a single SNP in the third exon of
197 *Hba-α1* and *Hba-α2* allows for variant calling analysis of the reads originating from the
198 α-globin transcripts. As in human, *Hba-α1* (the gene closest to the enhancers) accounted for
199 ~66% of the total α-globin mRNA and *Hba-α2* (the distal gene) accounted for ~34% (Figure
200 3a). Consistent with its higher level of expression, we have previously shown that the *Hba-α1*
201 promoter also preferentially interacts with the α-globin enhancers relative to the *Hba-α2*

bioRxiv preprint doi: https://doi.org/10.1101/2020.07.01.182089; this version posted July 1, 2020. The copyright holder for this preprint (which was not certified by peer review) is the author/funder, who has granted bioRxiv a license to display the preprint in perpetuity. It is made available under aCC-BY-NC-ND 4.0 International license.

202 promoter (40). As the θ CTCF sites are situated downstream of each α-globin gene (in the order
203 5'-α1-θ1-α2-θ2-3'), we investigated whether the θ CTCF sites, and in particular θ1 situated in
204 between the α-globin genes, regulate the differential expression of the mouse α-globin genes
205 and/or their interactions with the α-globin enhancers.
206
207 We first performed Poly(A)+ RNA-seq on primary erythroid cells isolated from Δθ1, Δθ2, and
208 Δθ1θ2 mice and used the variant calling analysis described above on the α-globin transcripts.
209 In all three models, the relative proportions of transcripts produced by *Hba-α1* and *Hba-α2*
210 were similar to that of WT (Figure 3a), showing that the loss of CTCF binding between and
211 downstream of the α-globin genes did not affect the preferential expression of *Hba-α1*. Next
212 we investigated whether the loss of CTCF binding around the α-globin genes altered
213 differential interactions of *Hba-α1/2* with the enhancers. From the Capture-C data analysed
214 from the viewpoints of the α-globin promoters in WT, Δθ2, and Δθ1θ2 primary erythroid cells
215 described above, we generated separate interaction profiles for the *Hba-α1* and *Hba-α2*
216 promoters following previously described analysis (40). When erythroid cells from Δθ2 and
217 Δθ1θ2 were analysed, we observed differential interaction profiles of the α-globin promoters
218 as previously reported in WT erythroid cells (Figure 3b,c). To investigate whether the loss of
219 CTCF binding between the α-globin promoters (at θ1) altered the differential interactions, we
220 generated comparisons of the *Hba-α1/2*-specific interaction profiles between Δθ2 and Δθ1θ2
221 erythroid cells. The only difference between these two models is the mutation at the θ1 site in
222 Δθ1θ2 mice. Again, there were no observable differences between the mutant mouse models
223 (Figure 3d), indicating that the differential interactions of *Hba-α1/2* with the enhancers is not
224 influenced by presence or absence of the θ1 CTCF site.
225
226 Therefore, in summary these findings suggest that CTCF binding at θ1 and/or θ2 do not
227 regulate the differential interactions of *Hba-α1/2* with the α-globin enhancers or the preferential
228 expression of the proximal α1-globin gene (*Hba-α1*) compared to the distal α2-globin gene
229 (*Hba-α2*). Rather, it appears that the transcribed α1-globin gene may act as a partial boundary
230 to the α2-globin gene in terms of access to a shared set of enhancers just as the α2-globin gene
231 acts as the downstream boundary of the sub-TAD.

bioRxiv preprint doi: https://doi.org/10.1101/2020.07.01.182089; this version posted July 1, 2020. The copyright holder for this preprint (which was not certified by peer review) is the author/funder, who has granted bioRxiv a license to display the preprint in perpetuity. It is made available under aCC-BY-NC-ND 4.0 International license.

232 **Discussion**

233

234 In many ways, the relatively small ~70 kb sub-TAD containing the mouse α-globin locus is
235 typical of other tissue-specific TADs or sub-TADs seen in mammalian genomes. The cluster
236 of erythroid-specific enhancers, which fulfil the definition of a super-enhancer (41), and the
237 promoters of the α-like genes, are flanked by largely convergent CTCF binding sites which are
238 often considered to act as the structural and functional boundaries of TADs. Current models
239 relating genome structure to function propose that TADs are formed by the extrusion of
240 chromatin loops as the cohesin complex translocates throughout the TAD (13-15). The
241 continuous process of extrusion ultimately brings together all sequences within the self-
242 interacting TAD, including the enhancers and promoters, providing the proximity thought to
243 be required for the activation of transcription. The borders of the TAD are created when cohesin
244 is stalled and stabilised by its interaction with the N-terminal region of CTCF. Our previous
245 studies of the mouse α-globin sub-TAD using chromosome conformation capture (26, 39-44)
246 and super-resolution imaging (39) are entirely consistent with this model involving the
247 interplay between enhancers, promoters, and boundary elements. Here, we have identified the
248 precise elements responsible for forming the boundaries of the sub-TAD and contributing to
249 the differential interactions between the enhancers and the promoters. Surprisingly, we find
250 that the transcriptionally active α-globin genes rather than the anticipated CTCF binding sites
251 play a role as boundary elements within the locus and in creating the downstream boundary of
252 the sub-TAD.

253

254 We have previously characterised the upstream 5’ boundary of the α-globin sub-TAD (26)
255 which is marked by two convergent CTCF binding sites (HS-38/-39 in Figure 1). Deletion of
256 these sites leads to extension of the sub-TAD to more distal flanking CTCF site (HS-59) and
257 erythroid-specific activation of three genes incorporated into the extended sub-TAD.
258 Presumably this occurs because the cohesin complex can now translocate beyond these sites.
259 Deletion of two CTCF sites (HS+44/+48) flanking the 3’ end of the α-globin locus which
260 interact with the upstream boundary behaved differently from those at the 5’ boundary.
261 Deletion of these sites led to only a very small increase in the levels of interaction with the
262 downstream flanking region beyond these sites, extending to the next CTCF sites
263 (HS+65/+66). However, there was no associated change in expression of the downstream
264 flanking genes (*Sh3pxd2b* and *Ubtd2*). In effect, removal of the HS+44/+48 sites caused no
265 change in the major transition (grey arrows in Figure 2) between interacting and non-

bioRxiv preprint doi: https://doi.org/10.1101/2020.07.01.182089; this version posted July 1, 2020. The copyright holder for this preprint (which was not certified by peer review) is the author/funder, who has granted bioRxiv a license to display the preprint in perpetuity. It is made available under aCC-BY-NC-ND 4.0 International license.

266 interacting chromatin. This major boundary coincides with the actively transcribed α2-globin
267 gene and/or a CTCF associated with the θ2-globin gene. Removal of this CTCF site did not
268 alter the predominant transition showing that it is the transcribed α-globin gene itself that
269 corresponds to the prominent 3' boundary of the sub-TAD.
270
271 Previous studies have identified between 15,000 and 40,000 CTCF binding sites in the genome
272 (49-53), but despite having common consensus sequences and chromatin signatures, only a
273 small proportion appear to act as boundary elements or to constrain the activity of enhancers
274 (8). A CTCF site lying between the mouse α1- and α2-globin genes appeared to provide an
275 example of an element which might partially block enhancer activity. The identical promoters
276 of the α1- and α2-globin genes interact differently with the enhancers and consequently direct
277 different levels of α-globin mRNA. However, deletion of the internal CTCF binding sites at
278 θ1/2 had no effect on the differential interactions of the two α-globin genes or the preferential
279 expression of the proximal α1-globin gene. This suggests that the α1-globin gene itself acts as
280 a partial boundary between the α2-globin gene and the α-globin enhancers.
281
282 Together, our findings on flanking and internal CTCF sites support the proposal that some
283 actively transcribed genes, in a particular context, may themselves behave as boundaries. One
284 mechanism by which this could occur is via competition between promoters and a shared
285 enhancer in a situation where there is unconstrained chromatin looping (Figure 4A). Such a
286 competition model would propose that the promoter of the α1-globin gene outcompetes that of
287 the α2-globin gene for access to the α-globin enhancers in which all enhancer elements appear
288 to act as a single entity (43). However, this seems unlikely since in the context of a freely
289 interacting chromosomal loop the promoters are located at a relatively similar distance from
290 the enhancer region and are identical in sequence. Similar examples of promoter competition
291 have also been proposed in which active promoters are located between an enhancer and
292 another, more distal promoter causing reduced activity of the distal promoter (54-57).
293
294 An alternative explanation proposes a *directional* tracking mechanism from enhancers to
295 promoters both of which have enriched levels of cohesin. Such a model of directional loop
296 extrusion has been proposed to explain interacting stripes seen in Hi-C maps (58). In this case
297 the anchor of the extruding loop would correspond to the HS-38/-39 sites. Multi-protein
298 complexes recruited to an actively transcribing gene might act, like a CTCF boundary, to stall
299 translocation of the cohesin complex and thereby reduce access of the enhancer to a more distal

bioRxiv preprint doi: https://doi.org/10.1101/2020.07.01.182089; this version posted July 1, 2020. The copyright holder for this preprint (which was not certified by peer review) is the author/funder, who has granted bioRxiv a license to display the preprint in perpetuity. It is made available under aCC-BY-NC-ND 4.0 International license.

300 promoter (Figure 4B). This interpretation of the mouse data presented here, is supported by
301 observations of the orthologous human and sheep α-globin clusters in which, the proximal
302 duplicated α-globin gene is also expressed in preference (~70 %) to the more distal gene
303 (~30%) (46-48, 59). In the human there is no CTCF binding site between the α-globin genes.
304 Of relevance, in both human and sheep with further tandem duplications producing
305 chromosomes with two (αα/), three (ααα/), four (αααα/), or five (ααααα/) almost identical
306 α-globin genes (59-62), each additional gene provides a smaller contribution to α-globin
307 mRNA and protein, as in a gradient. Furthermore, in humans, a deletion of the proximal
308 α2-globin gene (-α/) increases the output of the distal α1-globin gene from 20% to 50% (46).
309 By contrast, when there is an inactivating coding mutation in the proximal α2-globin gene
310 ($\alpha^{M}\alpha$/), leaving its promoter and transcription intact, RNA expression from the distal α1-globin
311 gene remains at 20% leading to the severe phenotype seen in patients with such nondeletional
312 mutations (63). A similar situation with a gradient in expression has also been observed for the
313 almost identical duplicated (γγ/), triplicated (γγγ/), and quadruplicated (γγγγ/) γ-globin genes
314 (64). The ratio of expression of the duplicated proximal to the distal γ-globin gene with respect
315 to the β-globin enhancers when they are active in fetal life is again ~70% to ~30% (65).
316
317 In this model highly transcribed genes might form a barrier to loop extrusion (66), due to
318 accumulation of large amounts of transcriptional machinery and regulatory factors. In these
319 scenarios, cohesin may be prevented from extruding chromatin loops due to the size of multi-
320 protein complexes which may be acting like 'roadblocks' via a passive blocking mechanism
321 (Figure 4B). Evidence that supports this comes from structural studies looking at the interaction
322 between CTCF and cohesin. The N terminus of CTCF structurally interacts with cohesin,
323 however, it appears its role is to stabilise cohesin on chromatin; when the N terminus is
324 mutated, cohesin still accumulates at CTCF sites but at lower levels compared to WT (67).
325 This suggests that CTCF is sufficient to block cohesin without a specific interaction and the
326 same could be true for other large proteins.
327
328 Therefore, there may be different methods to block loop extrusion; CTCF can directly interact
329 with cohesin causing it to be retained at CTCF-bound sites; however, passive blocking of
330 cohesin by large multi-protein complexes may also occur and could provide a mechanism for
331 how actively transcribed genes can behave as boundaries.
332

bioRxiv preprint doi: https://doi.org/10.1101/2020.07.01.182089; this version posted July 1, 2020. The copyright holder for this preprint (which was not certified by peer review) is the author/funder, who has granted bioRxiv a license to display the preprint in perpetuity. It is made available under aCC-BY-NC-ND 4.0 International license.

333 In summary, we provide evidence that in addition to CTCF binding sites, actively transcribed
334 genes may also behave as boundaries in agreement with studies that found that some TAD
335 boundaries are enriched for the promoters of actively transcribed genes, such as housekeeping
336 genes (8, 35). This suggests that an active promoter may have multiple roles in shaping the
337 genome.

bioRxiv preprint doi: https://doi.org/10.1101/2020.07.01.182089; this version posted July 1, 2020. The copyright holder for this preprint (which was not certified by peer review) is the author/funder, who has granted bioRxiv a license to display the preprint in perpetuity. It is made available under aCC-BY-NC-ND 4.0 International license.

338 **Methods**

339

340 Animal procedure

341 The mutant and wild-type mouse strains reported in this study were generated and maintained
342 on a C57BL/6J background in accordance with the European Union Directive 2010/63/EU
343 and/or the UK Animal (Scientific Procedures) Act 1986, with procedures reviewed by the
344 clinical medicine Animal Welfare and Ethical Review Body (AWERB). Experimental
345 procedures were conducted under project licences PPL 30/3339 and PAA2AAE49. All animals
346 were housed in Individually Ventilated Cages with enrichment, provided with food and water
347 *ad libitum*, and maintained on a 12 h light: 12 h dark cycle (150-200 lux cool white LED light,
348 measured at the cage floor). Mice were given neutral identifiers and analysed by research
349 technicians unaware of mouse genotype during outcome assessment.

350

351 Isolation of erythroid cells derived from adult mouse spleen

352 Primary Ter119+ erythroid cells were obtained from the spleens of adult mice that were treated
353 with phenylhydrazine as described previously (68). Spleens were mechanically dissociated into
354 single cells suspensions in cold phosphate-buffered saline (PBS; Gibco: 10010023)/10% fetal
355 bovine serum (FBS; Gibco: 10270106) and passed through a 70 μm filter to remove clumps.
356 Cells were washed with cold PBS/10% FBS and resuspended in 10 μl of cold PBS/10% FBS
357 per 10^6 cells and stained with a 1/100 dilution of anti-Ter119-PE antibody (Miltenyi Biotec:
358 130-102-336) at 4 °C for 20 minutes. Stained cells were washed with cold PBS/10% FBS and
359 resuspended in 8 μl of cold PBS/0.5% BSA/2 mM EDTA and 2 μl of anti-PE MACS
360 microbeads (Miltenyi Biotec: 130-048-801) per 10^6 cells and incubated at 4 °C for 15 minutes.
361 Ter119+ cells were positively selected via MACS lineage selection columns (Miltenyi Biotec:
362 130-042-401) and processed for downstream applications. Purity of the isolated erythroid cells
363 was routinely verified by Fluorescence-Activated Cell Sorting (FACS).

364

365 Generation of mutant mouse strains

366 Mouse models harbouring mutations of CTCF binding sites around the mouse α-globin locus
367 were generated using CRISPR-Cas9 mediated genome editing by either targeting mouse
368 embryonic stem cells, which were then used in blastocyst injections, or by direct microinjection
369 of zygotes. Preparation of CRISPR-Cas9 expression constructs for targeting of mouse
370 embryonic stem cells and preparation of CRISPR-Cas9 reagents and ssODN templates, as
371 required, for direct microinjection of zygotes were performed as previously described (26). The

bioRxiv preprint doi: https://doi.org/10.1101/2020.07.01.182089; this version posted July 1, 2020. The copyright holder for this preprint (which was not certified by peer review) is the author/funder, who has granted bioRxiv a license to display the preprint in perpetuity. It is made available under aCC-BY-NC-ND 4.0 International license.

372 20 nucleotide guide sequences used to direct the Cas9 protein to the target CTCF binding sites
373 and the ssODN donor sequences are shown in Supplementary Table 1.
374
375 ATAC-seq
376 ATAC-seq was performed on 75,000 Ter119+ cells isolated from phenylhydrazine-treated
377 mouse spleens as previously described (69). ATAC-seq libraries were sequenced on the
378 Illumina Nextseq platform using a 75-cycle paired-end kit (NextSeq 500/550 High Output Kit
379 v2.5: 20024906). Data were analysed using an in-house pipeline (70) which uses Bowtie (71)
380 to map reads to the mm9 mouse genome build. PCR duplicates were removed, and biological
381 replicates were normalised to Reads Per Kilobase per Million (RPKM) mapped reads using
382 deeptools bamCoverage (72). Mitochondrial DNA was excluded from the normalisation. For
383 visualisation, ATAC-seq data were averaged across three biological replicates.
384
385 ChIP-seq
386 CTCF Chromatin immunoprecipitation (ChIP) was performed on 1 x 10^7 Ter119+ erythroid
387 cells using a ChIP Assay Kit (Millipore: 17-295) according to the manufacturer's instructions.
388 Cells were crosslinked by a single 10 min 1% formaldehyde fixation. Chromatin fragmentation
389 was performed with the Bioruptor Pico sonicator (Diagenode) for a total sonication time of 4
390 min (8 cycles) at 4°C to obtain an average fragment size between 200 and 400 bp.
391 Immunoprecipitation was performed overnight at 4 °C with an anti-CTCF antibody (10 µl 07-
392 729, lot: 2836926; Millipore). Library preparation of immunoprecipitated DNA fragments was
393 performed using NEBNext Ultra II DNA Library Prep Kit for Illumina (New England Biolabs:
394 E7645) according to the manufacturer's instructions. Libraries were sequenced on the Illumina
395 Nextseq platform using either a 75-cycle paired-end kit (NextSeq 500/550 High Output Kit
396 v2.5: 20024906) or a 300-cycle paired-end kit (NextSeq 500/550 Mid Output Kit v2.5:
397 20024905). Data were analysed using an in-house pipeline (70) which uses Bowtie (71) to map
398 reads to the mm9 mouse genome build. PCR duplicates were removed, and biological
399 replicates were normalised to RPKM mapped reads using deeptools bamCoverage (72). For
400 visualisation, ChIP-seq data were averaged across three biological replicates.
401
402
403 NG Capture-C
404 Next-generation Capture-C was performed as previously described (40). A total of 1-2 x 10^7
405 Ter119+ erythroid cells were used per biological replicate. We prepared 3C libraries using the

bioRxiv preprint doi: https://doi.org/10.1101/2020.07.01.182089; this version posted July 1, 2020. The copyright holder for this preprint (which was not certified by peer review) is the author/funder, who has granted bioRxiv a license to display the preprint in perpetuity. It is made available under aCC-BY-NC-ND 4.0 International license.

406 DpnII-restriction enzyme for digestion. We added Illumina TruSeq adaptors using the
407 NEBNext Ultra II DNA Library Prep Kit for Illumina (New England Biolabs: E7645)
408 according to the manufacturer's instructions, and performed capture enrichment using
409 NimbleGen SeqCap EZ Hybridization and Wash Kit (Roche: 05634261001), NimbleGen
410 SeqCap EZ Accessory Kit v2 (Roche: 07145594001), and previously published custom
411 biotinylated DNA oligonucleotides (R1 and HS-38 viewpoints (26); α-globin promoters
412 viewpoints (40)). NG Capture-C data were analysed using the CaptureCompendium toolkit
413 (73) which uses Bowtie (71) to map reads to the mm9 mouse genome build. *Cis* reporter counts
414 for each sample were normalised to 100,000 reporters for calculation of the mean and standard
415 deviation (three biological replicates). Mean reporter counts were divided into 150 bp bins and
416 smoothed using a 3 kb window.
417
418 RNA expression analysis
419 Total RNA was isolated from 5 x 10^6 Ter119+ erythroid cells lysed in TRI reagent (Sigma-
420 Aldrich: T9424) using a Direct-zol RNA MiniPrep kit (Zymo Research: R2050). DNase I
421 treatment was performed on the column as recommended in the manufacturer's instructions
422 but with an increased incubation of 30 min at room temperature (rather than 15 min). To assess
423 relative changes in gene expression by qPCR, cDNA was synthesised from 1 µg of total RNA
424 using SuperScript III First-Strand Synthesis SuperMix for qRT-PCR (Invitrogen,
425 ThermoFisher: 11752-050) according to the manufacturer's instructions. The ΔΔCt method
426 was used for relative quantification of RNA abundance using TaqMan Universal PCR Master
427 Mix (Applied Biosystems, ThermoFisher: 4304437) and the following TaqMan probes:
428 Mm00845395_s1 (*Hba-α1/2*), Mm01611268_g1 (*Hbb-b1*), Mm00616672_m1 (*Sh3pxd2b*),
429 Mm00612868_m1 (*Ubtd2*), and Mm04277571_s1 (*Rn18s*). For RNA-seq libraries, 1-2 µg of
430 total RNA was depleted of rRNA and globin mRNA using the Globin-Zero Gold rRNA
431 Removal Kit (Illumina: GZG1224) according to the manufacturer's instructions. To enrich for
432 mRNA, poly(A)+ RNA was isolated, strand-specific cDNA was synthesised, and the resulting
433 libraries prepared for Illumina sequencing using the NEBNext Poly(A) mRNA Magnetic
434 Isolation Module (New England Biolabs: E7490) and the NEBNext Ultra II Directional RNA
435 Library Prep Kit for Illumina (New England Biolabs: E7760) following the manufacturer's
436 instructions. Poly(A)+ RNA-seq libraries were sequenced on the Illumina Nextseq platform
437 using a 75-cycle paired-end kit (NextSeq 500/550 High Output Kit v2.5: 20024906). Reads
438 were aligned to the mm9 mouse genome build using STAR (74). To perform variant calling
439 analysis on RNA-seq reads originating from α-globin transcripts an in-house variant-caller tool

bioRxiv preprint doi: https://doi.org/10.1101/2020.07.01.182089; this version posted July 1, 2020. The copyright holder for this preprint (which was not certified by peer review) is the author/funder, who has granted bioRxiv a license to display the preprint in perpetuity. It is made available under aCC-BY-NC-ND 4.0 International license.

440 developed by Jelena Telenius was used, which was based on the samtools1 version of mpileup
441 (75) to count variants. Each sample was aligned twice to the mouse mm9 genome: once with
442 *Hba-α1* masked and once with *Hba-α2* masked. The resulting alignments were used as inputs
443 for the variant-caller which counted mismatches at *Hba-α1/2*. Full documentation for the
444 variant-caller tool can be found here:
445 http://userweb.molbiol.ox.ac.uk/public/telenius/variantApp/variantApp_JTelenius_GPL3_20
446 19.pdf.
447
448
449 **Data availability**
450
451 All sequencing data have been submitted to the NCBI Gene Expression Omnibus under
452 accession number GSE153209.

bioRxiv preprint doi: https://doi.org/10.1101/2020.07.01.182089; this version posted July 1, 2020. The copyright holder for this preprint (which was not certified by peer review) is the author/funder, who has granted bioRxiv a license to display the preprint in perpetuity. It is made available under aCC-BY-NC-ND 4.0 International license.

References

1. M. S. Kowalczyk *et al.*, Intragenic enhancers act as alternative promoters. *Mol Cell* **45**, 447-458 (2012).
2. O. Mikhaylichenko *et al.*, The degree of enhancer or promoter activity is reflected by the levels and directionality of eRNA transcription. *Genes Dev* **32**, 42-57 (2018).
3. T. A. Nguyen *et al.*, High-throughput functional comparison of promoter and enhancer activities. *Genome Res* **26**, 1023-1033 (2016).
4. J. van Arensbergen *et al.*, Genome-wide mapping of autonomous promoter activity in human cells. *Nat Biotechnol* **35**, 145-153 (2017).
5. C. D. Arnold *et al.*, Genome-wide quantitative enhancer activity maps identified by STARR-seq. *Science* **339**, 1074-1077 (2013).
6. L. T. M. Dao *et al.*, Genome-wide characterization of mammalian promoters with distal enhancer functions. *Nat Genet* **49**, 1073-1081 (2017).
7. M. A. Zabidi *et al.*, Enhancer-core-promoter specificity separates developmental and housekeeping gene regulation. *Nature* **518**, 556-559 (2015).
8. J. R. Dixon *et al.*, Topological domains in mammalian genomes identified by analysis of chromatin interactions. *Nature* **485**, 376-380 (2012).
9. E. P. Nora *et al.*, Spatial partitioning of the regulatory landscape of the X-inactivation centre. *Nature* **485**, 381-385 (2012).
10. J. E. Phillips-Cremins *et al.*, Architectural protein subclasses shape 3D organization of genomes during lineage commitment. *Cell* **153**, 1281-1295 (2013).
11. S. S. Rao *et al.*, A 3D map of the human genome at kilobase resolution reveals principles of chromatin looping. *Cell* **159**, 1665-1680 (2014).
12. T. Sexton *et al.*, Three-dimensional folding and functional organization principles of the Drosophila genome. *Cell* **148**, 458-472 (2012).
13. G. Fudenberg, N. Abdennur, M. Imakaev, A. Goloborodko, L. A. Mirny, Emerging Evidence of Chromosome Folding by Loop Extrusion. *Cold Spring Harb Symp Quant Biol* **82**, 45-55 (2017).
14. G. Fudenberg *et al.*, Formation of Chromosomal Domains by Loop Extrusion. *Cell Rep* **15**, 2038-2049 (2016).
15. A. L. Sanborn *et al.*, Chromatin extrusion explains key features of loop and domain formation in wild-type and engineered genomes. *Proc Natl Acad Sci U S A* **112**, E6456-6465 (2015).
16. S. Hadjur *et al.*, Cohesins form chromosomal cis-interactions at the developmentally regulated IFNG locus. *Nature* **460**, 410-413 (2009).
17. V. Parelho *et al.*, Cohesins functionally associate with CTCF on mammalian chromosome arms. *Cell* **132**, 422-433 (2008).
18. E. D. Rubio *et al.*, CTCF physically links cohesin to chromatin. *Proc Natl Acad Sci U S A* **105**, 8309-8314 (2008).
19. W. Stedman *et al.*, Cohesins localize with CTCF at the KSHV latency control region and at cellular c-myc and H19/Igf2 insulators. *Embo j* **27**, 654-666 (2008).
20. K. S. Wendt *et al.*, Cohesin mediates transcriptional insulation by CCCTC-binding factor. *Nature* **451**, 796-801 (2008).
21. E. de Wit *et al.*, CTCF Binding Polarity Determines Chromatin Looping. *Mol Cell* **60**, 676-684 (2015).
22. J. M. Dowen *et al.*, Control of cell identity genes occurs in insulated neighborhoods in mammalian chromosomes. *Cell* **159**, 374-387 (2014).
23. W. A. Flavahan *et al.*, Insulator dysfunction and oncogene activation in IDH mutant gliomas. *Nature* **529**, 110-114 (2016).
24. C. Gomez-Marin *et al.*, Evolutionary comparison reveals that diverging CTCF sites are signatures of ancestral topological associating domains borders. *Proc Natl Acad Sci U S A* **112**, 7542-7547 (2015).

bioRxiv preprint doi: https://doi.org/10.1101/2020.07.01.182089; this version posted July 1, 2020. The copyright holder for this preprint (which was not certified by peer review) is the author/funder, who has granted bioRxiv a license to display the preprint in perpetuity. It is made available under aCC-BY-NC-ND 4.0 International license.

25. Y. Guo *et al.*, CRISPR Inversion of CTCF Sites Alters Genome Topology and Enhancer/Promoter Function. *Cell* **162**, 900-910 (2015).
26. L. L. P. Hanssen *et al.*, Tissue-specific CTCF-cohesin-mediated chromatin architecture delimits enhancer interactions and function in vivo. *Nat Cell Biol* **19**, 952-961 (2017).
27. D. Hnisz *et al.*, Activation of proto-oncogenes by disruption of chromosome neighborhoods. *Science* **351**, 1454-1458 (2016).
28. D. G. Lupiáñez *et al.*, Disruptions of topological chromatin domains cause pathogenic rewiring of gene-enhancer interactions. *Cell* **161**, 1012-1025 (2015).
29. V. Narendra, M. Bulajic, J. Dekker, E. O. Mazzoni, D. Reinberg, CTCF-mediated topological boundaries during development foster appropriate gene regulation. *Genes Dev* **30**, 2657-2662 (2016).
30. V. Narendra *et al.*, CTCF establishes discrete functional chromatin domains at the Hox clusters during differentiation. *Science* **347**, 1017-1021 (2015).
31. A. R. Barutcu, P. G. Maass, J. P. Lewandowski, C. L. Weiner, J. L. Rinn, A TAD boundary is preserved upon deletion of the CTCF-rich Firre locus. *Nat Commun* **9**, 1444 (2018).
32. J. Hyle *et al.*, Acute depletion of CTCF directly affects MYC regulation through loss of enhancer-promoter looping. *Nucleic Acids Res* **47**, 6699-6713 (2019).
33. E. P. Nora *et al.*, Targeted Degradation of CTCF Decouples Local Insulation of Chromosome Domains from Genomic Compartmentalization. *Cell* **169**, 930-944.e922 (2017).
34. G. Wutz *et al.*, Topologically associating domains and chromatin loops depend on cohesin and are regulated by CTCF, WAPL, and PDS5 proteins. *Embo j* **36**, 3573-3599 (2017).
35. S. Hong, D. Kim, Computational characterization of chromatin domain boundary-associated genomic elements. *Nucleic Acids Res* **45**, 10403-10414 (2017).
36. A. R. Barutcu, B. J. Blencowe, J. L. Rinn, Differential contribution of steady-state RNA and active transcription in chromatin organization. *EMBO Rep* **20**, e48068 (2019).
37. G. A. Busslinger *et al.*, Cohesin is positioned in mammalian genomes by transcription, CTCF and Wapl. *Nature* **544**, 503-507 (2017).
38. S. Heinz *et al.*, Transcription Elongation Can Affect Genome 3D Structure. *Cell* **174**, 1522-1536 e1522 (2018).
39. J. M. Brown *et al.*, A tissue-specific self-interacting chromatin domain forms independently of enhancer-promoter interactions. *Nat Commun* **9**, 3849 (2018).
40. J. O. Davies *et al.*, Multiplexed analysis of chromosome conformation at vastly improved sensitivity. *Nat Methods* **13**, 74-80 (2016).
41. D. Hay *et al.*, Genetic dissection of the alpha-globin super-enhancer in vivo. *Nat Genet* **48**, 895-903 (2016).
42. A. M. Oudelaar & R. A. Beagrie *et al.*, Dynamics of the 4D genome during in vivo lineage specification and differentiation. *Nature Communications* **11**, 2722 (2020).
43. A. M. Oudelaar *et al.*, Single-allele chromatin interactions identify regulatory hubs in dynamic compartmentalized domains. *Nat Genet* **50**, 1744-1751 (2018).
44. A. M. Oudelaar & C. L. Harrold *et al.*, A revised model for promoter competition based on multi-way chromatin interactions at the α-globin locus. *Nat Commun* **10**, 5412 (2019).
45. S. L. Hsu *et al.*, Structure and expression of the human theta 1 globin gene. *Nature* **331**, 94-96 (1988).
46. S. A. Liebhaber, F. E. Cash, D. M. Main, Compensatory increase in alpha 1-globin gene expression in individuals heterozygous for the alpha-thalassemia-2 deletion. *J Clin Invest* **76**, 1057-1064 (1985).
47. S. A. Liebhaber, Y. W. Kan, Differentiation of the mRNA transcripts originating from the alpha 1- and alpha 2-globin loci in normals and alpha-thalassemics. *J Clin Invest* **68**, 439-446 (1981).
48. S. H. Orkin, S. C. Goff, The duplicated human alpha-globin genes: their relative expression as measured by RNA analysis. *Cell* **24**, 345-351 (1981).
49. S. Cuddapah *et al.*, Global analysis of the insulator binding protein CTCF in chromatin barrier regions reveals demarcation of active and repressive domains. *Genome Res* **19**, 24-32 (2009).
50. T. H. Kim *et al.*, Analysis of the vertebrate insulator protein CTCF-binding sites in the human genome. *Cell* **128**, 1231-1245 (2007).

bioRxiv preprint doi: https://doi.org/10.1101/2020.07.01.182089; this version posted July 1, 2020. The copyright holder for this preprint (which was not certified by peer review) is the author/funder, who has granted bioRxiv a license to display the preprint in perpetuity. It is made available under aCC-BY-NC-ND 4.0 International license.

51. H. Nakahashi *et al.*, A genome-wide map of CTCF multivalency redefines the CTCF code. *Cell Rep* **3**, 1678-1689 (2013).
52. D. Schmidt *et al.*, A CTCF-independent role for cohesin in tissue-specific transcription. *Genome Res* **20**, 578-588 (2010).
53. H. Wang *et al.*, Widespread plasticity in CTCF occupancy linked to DNA methylation. *Genome Res* **22**, 1680-1688 (2012).
54. C. R. Bartman, S. C. Hsu, C. C. Hsiung, A. Raj, G. A. Blobel, Enhancer Regulation of Transcriptional Bursting Parameters Revealed by Forced Chromatin Looping. *Mol Cell* **62**, 237-247 (2016).
55. S. W. Cho *et al.*, Promoter of lncRNA Gene PVT1 Is a Tumor-Suppressor DNA Boundary Element. *Cell* **173**, 1398-1412.e1322 (2018).
56. M. De Gobbi *et al.*, A regulatory SNP causes a human genetic disease by creating a new transcriptional promoter. *Science* **312**, 1215-1217 (2006).
57. M. Wijgerde, F. Grosveld, P. Fraser, Transcription complex stability and chromatin dynamics in vivo. *Nature* **377**, 209-213 (1995).
58. L. Vian *et al.*, The Energetics and Physiological Impact of Cohesin Extrusion. *Cell* **173**, 1165-1178.e1120 (2018).
59. R. Vestri, E. Pieragostini, M. S. Ristaldi, Expression gradient in sheep alpha alpha and alpha alpha alpha globin gene haplotypes: mRNA levels. *Blood* **83**, 2317-2322 (1994).
60. R. J. Cook, J. D. Hoyer, W. E. Highsmith, Quintuple alpha-globin gene: a novel allele in a Sudanese man. *Hemoglobin* **30**, 51-55 (2006).
61. Y. C. Gu, H. Landman, T. H. Huisman, Two different quadruplicated alpha globin gene arrangements. *Br J Haematol* **66**, 245-250 (1987).
62. D. R. Higgs, J. M. Old, L. Pressley, J. B. Clegg, D. J. Weatherall, A novel alpha-globin gene arrangement in man. *Nature* **284**, 632-635 (1980).
63. C. L. Harteveld, D. R. Higgs, Alpha-thalassaemia. *Orphanet J Rare Dis* **5**, 13 (2010).
64. S. Shimasaki, I. Iuchi, Diversity of human gamma-globin gene loci including a quadruplicated arrangement. *Blood* **67**, 784-788 (1986).
65. T. H. Huisman, W. A. Schroeder, A. Felice, D. Powars, B. Ringelhann, Anomaly in the gamma chain heterogeneity of the newborn. *Nature* **265**, 63-65 (1977).
66. H. B. Brandão *et al.*, RNA polymerases as moving barriers to condensin loop extrusion. *Proceedings of the National Academy of Sciences* **116**, 20489-20499 (2019).
67. Y. Li *et al.*, The structural basis for cohesin-CTCF-anchored loops. *Nature* **578**, 472-476 (2020).
68. J. L. Spivak, D. Toretti, H. W. Dickerman, Effect of phenylhydrazine-induced hemolytic anemia on nuclear RNA polymerase activity of the mouse spleen. *Blood* **42**, 257-266 (1973).
69. J. D. Buenrostro, P. G. Giresi, L. C. Zaba, H. Y. Chang, W. J. Greenleaf, Transposition of native chromatin for fast and sensitive epigenomic profiling of open chromatin, DNA-binding proteins and nucleosome position. *Nat Methods* **10**, 1213-1218 (2013).
70. J. Telenius, J. R. Hughes, NGseqBasic - a single-command UNIX tool for ATAC-seq, DNaseI-seq, Cut-and-Run, and ChIP-seq data mapping, high-resolution visualisation, and quality control. *bioRxiv* 10.1101/393413, 393413 (2018).
71. B. Langmead, C. Trapnell, M. Pop, S. L. Salzberg, Ultrafast and memory-efficient alignment of short DNA sequences to the human genome. *Genome Biol* **10**, R25 (2009).
72. F. Ramírez *et al.*, deepTools2: a next generation web server for deep-sequencing data analysis. *Nucleic Acids Res* **44**, W160-165 (2016).
73. J. M. Telenius *et al.*, CaptureCompendium: a comprehensive toolkit for 3C analysis. *bioRxiv* 10.1101/2020.02.17.952572, 2020.2002.2017.952572 (2020).
74. A. Dobin *et al.*, STAR: ultrafast universal RNA-seq aligner. *Bioinformatics* **29**, 15-21 (2013).
75. H. Li *et al.*, The Sequence Alignment/Map format and SAMtools. *Bioinformatics* **25**, 2078-2079 (2009).

bioRxiv preprint doi: https://doi.org/10.1101/2020.07.01.182089; this version posted July 1, 2020. The copyright holder for this preprint (which was not certified by peer review) is the author/funder, who has granted bioRxiv a license to display the preprint in perpetuity. It is made available under aCC-BY-NC-ND 4.0 International license.

Acknowledgements

This work was supported by Wellcome (Genomic Medicine and Statistics PhD Programme, reference 109110/Z/15/Z; Chromosome and Developmental Biology PhD Programme, reference 099684/Z/12/Z; Wellcome Trust Strategic Award, reference 106130/Z/14/Z; Wellcome Trust Core Award, reference 203141/Z/16/Z) and the Medical Research Council (MRC Core Funding and Project Grant, reference MR/N00969X/1).

Author contributions

C.L.H., L.L.P.H., B.D., M.T.K., J.R.H. and D.R.H conceived and designed experiments and coordinated and advised on the project. C.L.H., M.E.G. and R.J.S. performed experiments. C.L.H., D.J.D. and J.M.T performed bioinformatic analyses. D.B., C.P., S.A., J.A.S. and J.A.S.-S. generated essential reagents and carried out mice maintenance. C.L.H. and D.R.H. wrote the manuscript. J.R.H. and D.R.H. supervised works carried out.

Competing interests

J.R.H is a founder and shareholder of Nucleome Therapeutics.

bioRxiv preprint doi: https://doi.org/10.1101/2020.07.01.182089; this version posted July 1, 2020. The copyright holder for this preprint (which was not certified by peer review) is the author/funder, who has granted bioRxiv a license to display the preprint in perpetuity. It is made available under aCC-BY-NC-ND 4.0 International license.

Figure 1: Characterisation of the deletion of CTCF-bound sites downstream of the α-globin locus

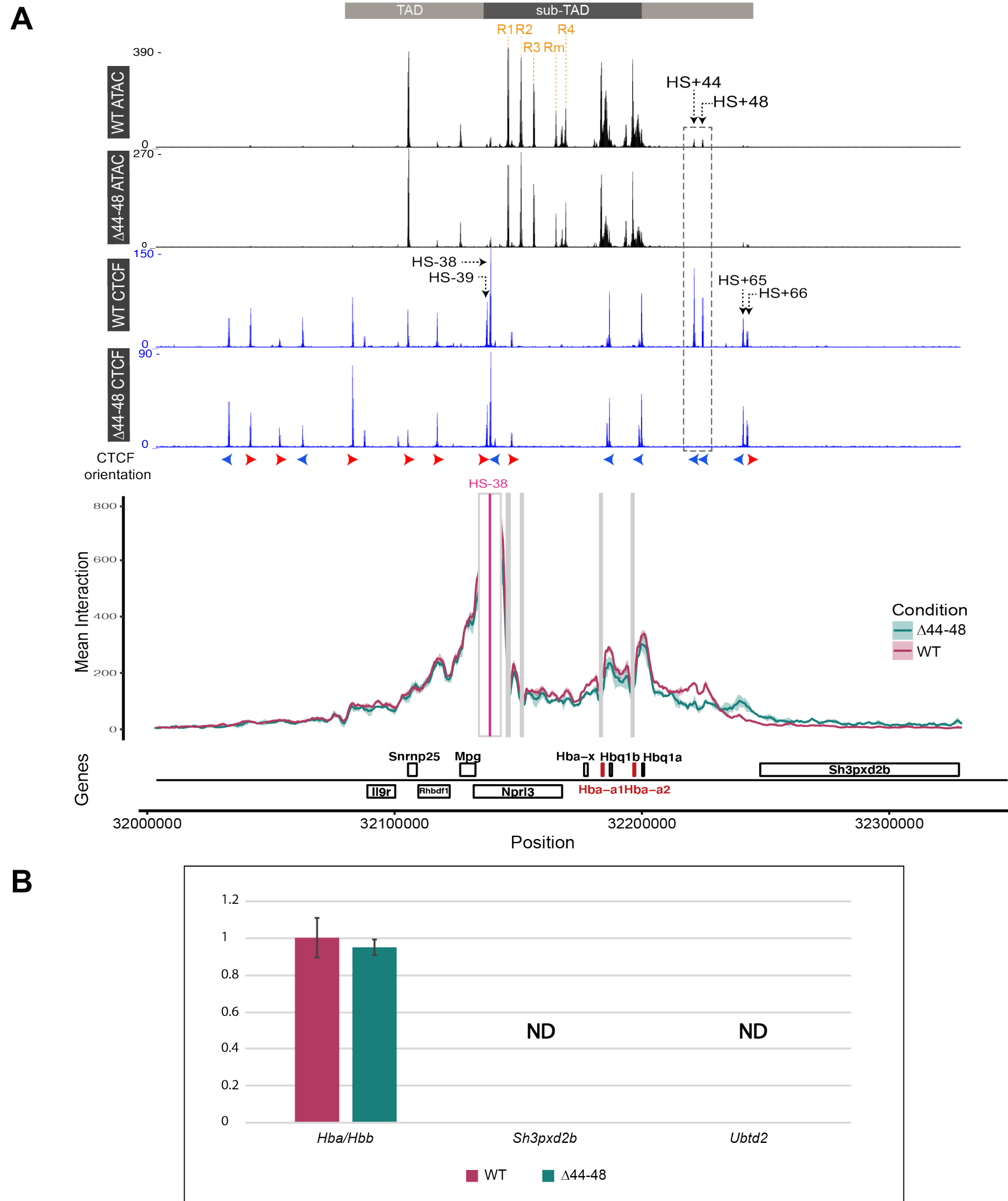

A: Top tracks show profiles for ATAC-seq and CTCF ChIP-seq in primary erythroid cells isolated from WT (26) and Δ44-48 mice (Ter119+) for the α-globin locus on chromosome 11. Profiles show normalised (RPKM) and averaged data from three biological replicates. The individual α-globin enhancer elements are highlighted in orange (R1-R4 & Rm). The horizontal grey bars above the tracks

bioRxiv preprint doi: https://doi.org/10.1101/2020.07.01.182089; this version posted July 1, 2020. The copyright holder for this preprint (which was not certified by peer review) is the author/funder, who has granted bioRxiv a license to display the preprint in perpetuity. It is made available under aCC-BY-NC-ND 4.0 International license.

represent the ~70 kb α-globin sub-TAD (dark grey) nested within a larger ~165 kb TAD (light grey). The orientation of CTCF motifs is shown under peaks by red (forward) and blue (reverse) arrows. NG Capture-C interaction profiles of the α-globin locus from the viewpoint of HS-38 (pink), with a 1 kb exclusion zone around the viewpoint, in WT (red) and Δ44-48 (green) Ter119+ primary erythroid cells. The profiles represent normalised and averaged unique interactions from three biological replicates, with the halo representing the standard deviation of a sliding 3 kb window. Vertical grey bars denote other capture points included in this experiment. Genes and genomic position below interaction profiles, with positioning of genes above or below the line representing sense (above) and antisense (below) transcription. The α-globin genes are highlighted in red.
B: Reverse transcription qPCR expression analysis of α- and β-globin mRNA ratio, *Sh3pxd2b* mRNA, and *Ubtd2* mRNA in WT (red) and Δ44-48 (green) Ter119+ erythroid cells, normalised to 18S RNA. Mean and standard deviation of three biological replicates shown. Data normalised to WT.

bioRxiv preprint doi: https://doi.org/10.1101/2020.07.01.182089; this version posted July 1, 2020. The copyright holder for this preprint (which was not certified by peer review) is the author/funder, who has granted bioRxiv a license to display the preprint in perpetuity. It is made available under aCC-BY-NC-ND 4.0 International license.

Figure 2: Deletion of CTCF-bound sites leaves the 3' boundary of the α-globin sub-TAD largely intact

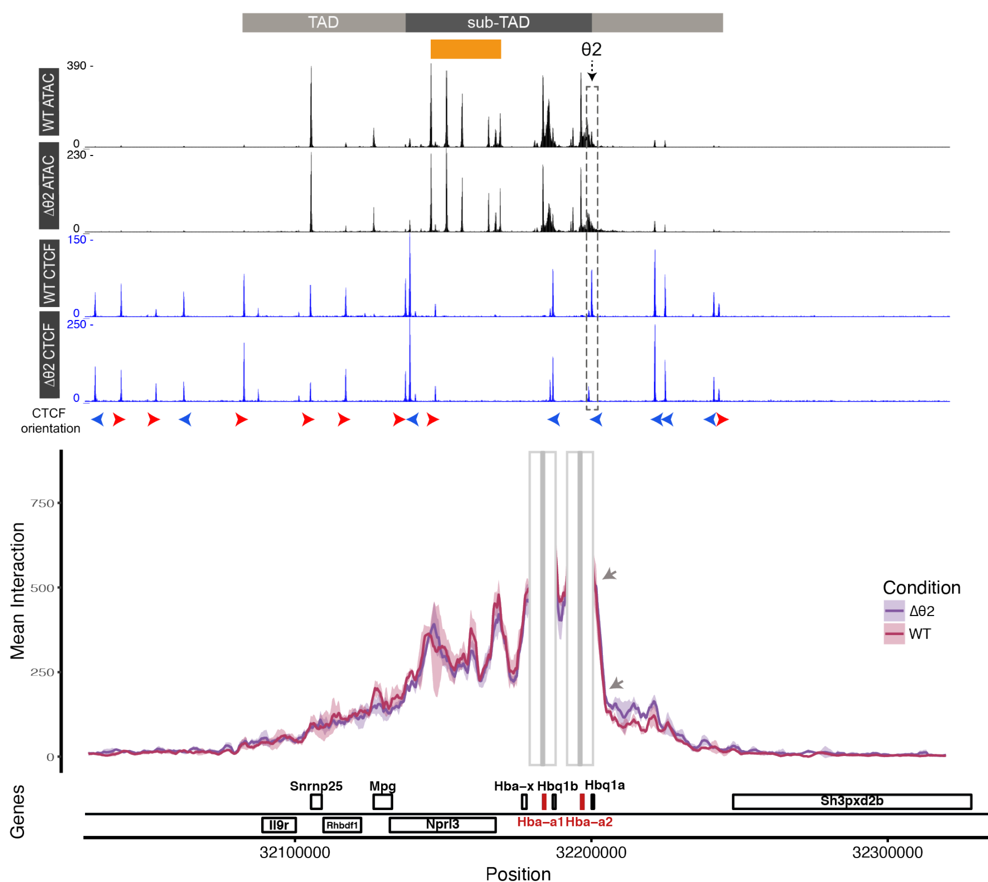

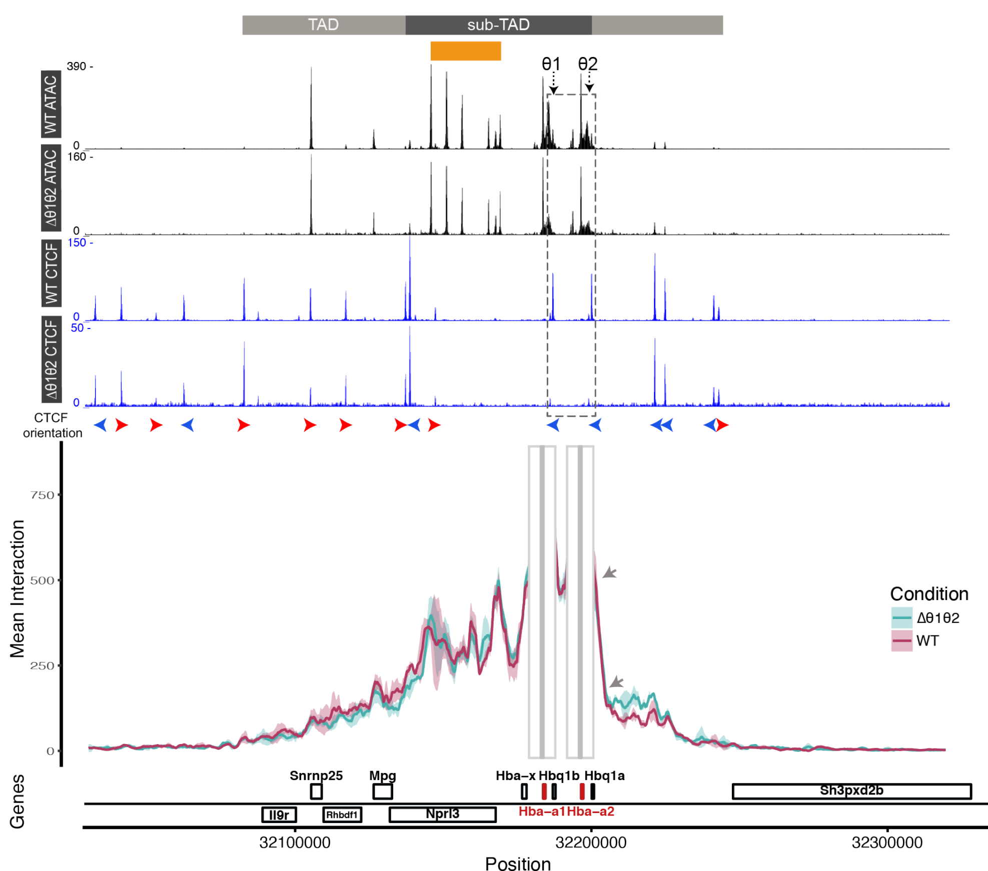

bioRxiv preprint doi: https://doi.org/10.1101/2020.07.01.182089; this version posted July 1, 2020. The copyright holder for this preprint (which was not certified by peer review) is the author/funder, who has granted bioRxiv a license to display the preprint in perpetuity. It is made available under aCC-BY-NC-ND 4.0 International license.

Interaction profiles from the combined viewpoints of the α-globin promoters in Δθ2 (**A**) and Δθ1θ2 (**B**) erythroid cells.

In **A**, **B**: Top tracks show profiles for ATAC-seq and CTCF ChIP-seq in primary erythroid cells isolated from WT (26) and the respective mouse model (Ter119+) for the α-globin locus on chromosome 11. Profiles show normalised (RPKM) and averaged data from three biological replicates. The α-globin enhancer region is represented by an orange box. The horizontal grey bars above the tracks represent the ~70 kb α-globin sub-TAD (dark grey) nested within a larger ~165 kb TAD (light grey). The orientation of CTCF motifs is shown under peaks by red (forward) and blue (reverse) arrows. NG Capture-C interaction profiles of the α-globin locus from the viewpoints of the α-globin promoters (grey), with a 1 kb exclusion zone around the viewpoints, in WT (red), Δθ2 (purple), and Δθ1θ2 (teal) Ter119+ primary erythroid cells. The profiles represent normalised and averaged unique interactions from three biological replicates, with the halo representing the standard deviation of a sliding 3kb window. Grey arrows denote the 3' edge of the α-globin sub-TAD. Genes and genomic position below interaction profiles, with positioning of genes above or below the line representing sense (above) and antisense (below) transcription. The α-globin genes are highlighted in red.

bioRxiv preprint doi: https://doi.org/10.1101/2020.07.01.182089; this version posted July 1, 2020. The copyright holder for this preprint (which was not certified by peer review) is the author/funder, who has granted bioRxiv a license to display the preprint in perpetuity. It is made available under aCC-BY-NC-ND 4.0 International license.

Figure 3: CTCF does not regulate the differential interactions and expression of the α-globin genes

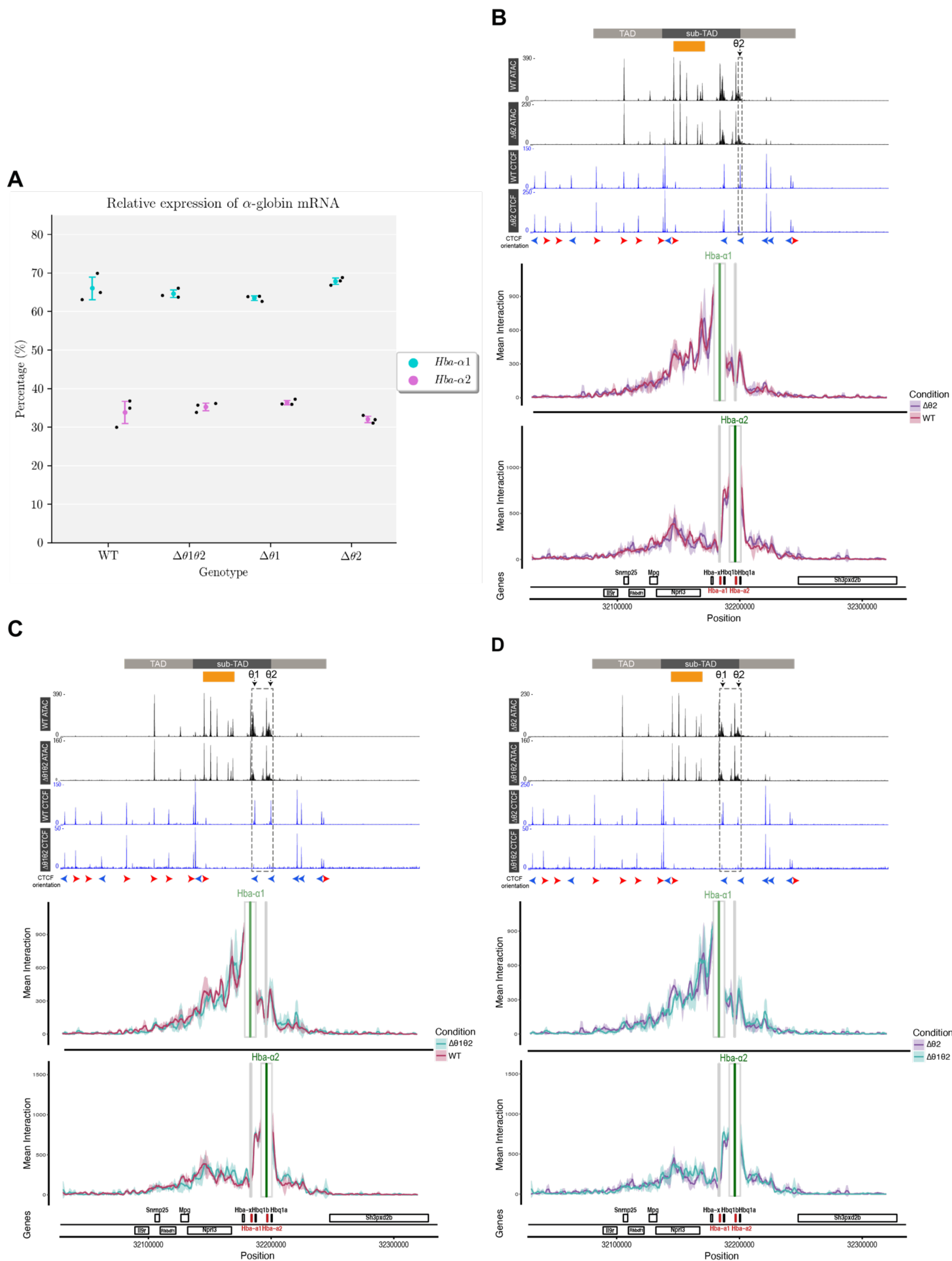

bioRxiv preprint doi: https://doi.org/10.1101/2020.07.01.182089; this version posted July 1, 2020. The copyright holder for this preprint (which was not certified by peer review) is the author/funder, who has granted bioRxiv a license to display the preprint in perpetuity. It is made available under aCC-BY-NC-ND 4.0 International license.

A: Relative expression of *Hba-α1/2* mRNA in WT, Δθ1θ2, Δθ1, and Δθ2 primary erythroid cells (Ter119+). Variant calling analysis performed on Poly(A)+ RNA-seq data from biological triplicates revealed percentage of reads originating from transcripts of *Hba-α1* (teal) or *Hba-α2* (pink). Mean and standard deviation for each model shown, and each point represents a biological replicate.
B: Effects of the deletion of θ2 on local chromatin accessibility, CTCF binding, and *Hba-α1/2*-specific interaction profiles.
C: Effects of the combined deletion of θ1and θ2 on local chromatin accessibility, CTCF binding, and *Hba-α1/2*-specific interaction profiles.
D: Comparison of *Hba-α1/*2-specific interaction profiles in Δθ2 and Δθ1θ2 erythroid cells.
In **A**, **B**, **C**: Top tracks show profiles for ATAC-seq and CTCF ChIP-seq in primary erythroid cells isolated from WT (26) and the respective mouse model (Ter119+) for the α-globin locus on chromosome 11. Profiles show normalised (RPKM) and averaged data from three biological replicates. The α-globin enhancer region is represented by an orange box. The horizontal grey bars above the tracks represent the ~70 kb α-globin sub-TAD (dark grey) nested within a larger ~165 kb TAD (light grey). The orientation of CTCF motifs is shown under peaks by red (forward) and blue (reverse) arrows. NG Capture-C interaction profiles of the α-globin locus from the viewpoints of the α-globin promoters (*Hba-α1* in light green; *Hba-α2* in dark green), with a 1 kb exclusion zone around the viewpoints, in WT (red), Δθ2 (purple), and Δθ1θ2 (teal) Ter119+ primary erythroid cells. The profiles represent normalised and averaged unique interactions from three biological replicates, with the halo representing the standard deviation of a sliding 3 kb window. Genes and genomic position below interaction profiles, with positioning of genes above or below the line representing sense (above) and antisense (below) transcription. The α-globin genes are highlighted in red.

bioRxiv preprint doi: https://doi.org/10.1101/2020.07.01.182089; this version posted July 1, 2020. The copyright holder for this preprint (which was not certified by peer review) is the author/funder, who has granted bioRxiv a license to display the preprint in perpetuity. It is made available under aCC-BY-NC-ND 4.0 International license.

Figure 4: Proposed mechanisms for actively transcribed genes behaving as boundary elements

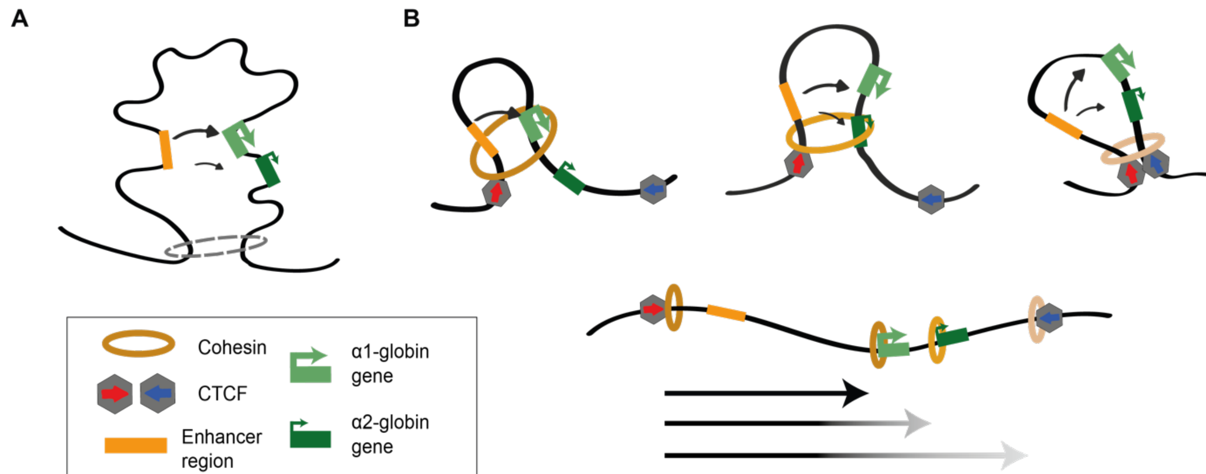

A: Schematic to show that under unconstrained chromatin looping, the α1-globin gene outcompetes the α2-globin gene via promoter competition for access to the shared set of α-globin enhancers.
B: Schematic to show a dynamic, directional tracking mechanism of chromatin loop extrusion by cohesin from the α-globin enhancers to the promoters. Multi-protein complexes recruited to the actively transcribing genes stall cohesin translocation on chromatin resulting in cohesin retention at active genes, in addition to CTCF binding sites.